NOAA Technical Memorandum NMFS

CALIBRATIONS OF WIDE-BANDWIDTH TRANSCEIVERS (WBT MINI) WITH DUAL-FREQUENCY TRANSDUCERS (ES38-18/200-18C) FOR SAILDRONE SURVEYS OF THE CALIFORNIA CURRENT ECOSYSTEM DURING SUMMER 2018

Josiah S. Renfree, Thomas S. Sessions, David Murfin, Danial G. Palance, and David A. Demer

NOAA Fisheries
SWFSC Fisheries Resources Division
8901 La Jolla Shores Drive
La Jolla, CA 92037

About the NOAA Technical Memorandum series

The National Oceanic and Atmospheric Administration (NOAA), organized in 1970, has evolved into an agency which establishes national policies and manages and conserves our oceanic, coastal, and atmospheric resources. An organizational element within NOAA, the Office of Fisheries is responsible for fisheries policy and the direction of the National Marine Fisheries Service (NMFS).

In addition to its formal publications, the NMFS uses the NOAA Technical Memorandum series to issue informal scientific and technical publications when complete formal review and editorial processing are not appropriate or feasible. Documents within this series, however, reflect sound professional work and may be referenced in the formal scientific and technical literature.

SWFSC Technical Memorandums are available online at the following websites:

Southwest Fisheries Science Center

NOAA Repository

NTIS National Technical Reports Library

Accessibility information

NOAA Fisheries Southwest Fisheries Science Center (SWFSC) is committed to making our publications and supporting electronic documents accessible to individuals of all abilities. The complexity of some of SWFSC's publications, information, data, and products may make access difficult for some. If you encounter material in this document that you cannot access or use, please contact us so that we may assist you.
Phone: 858-546-7000

Terms, Symbols, and Units

The terms and symbols used throughout this report are based on recommendations from MacLennan et al. (2002) and Demer et al. (2015).

Term	Symbol	Unit	Description
Transducer electrical impedance	z_{et}	Ω	The ability of a transducer to oppose the passage of an alternating electric current.
Transducer electrical conductance	G	S	The ability of a transducer to conduct the passage of an alternating electric current.
Transducer electrical phase	φ	°	Relative phase between the voltage and current passing through a transducer.
Target Strength	TS	dB re 1 m^2	The area of an acoustic target effectively backscattering acoustic power.
On-axis Target Strength	$TS_{\mathrm{on-axis}}$	dB re 1 m^2	The TS of a target located approximately in the center of the transducer beam axis.
Volume backscattering strength	S_{V}	dB re 1 m^2 m^{-3}	The sum of the area of an acoustic target effectively backscattering acoustic power per unit of water volume.
Directional angles	α, β	°	The angle coordinates in orthogonal planes, typically alongships and athwartships or aligned with the minor and major transducer axes, respectively.
Transducer electrical angle	$\theta_{e\alpha}$ or $\theta_{e\beta}$	Electrical°	Electrical phase angle between signals received in the α or β plans.
Transducer angle sensitivity	Λ_{α} or Λ_{β}	Electrical°/geometric°	A factor to convert split-beam electrical angles to target bearing angles in the α or β planes.
Transducer beamwidth	$\alpha_{-3\,\mathrm{dB}}$ or $\beta_{-3\,\mathrm{dB}}$	°	The angle from the transducer beam axis to the point of half-power in the α or β planes.
Target range	r	m	The direct-path distance between the transducer and a target.

Term	Symbol	Unit	Description
Effective transducer separation	d_α or d_β	m	Distance, in the α or β planes, between the effective centers of two collocated transducers.
On-axis gain	g_0 or G_0	Dimensionless or dB re 1	The ratio of intensity on the beam axis, observed at a distant point, resulting from transmissions of a real transducer with constant transmit power, and an idealized lossless omnidirectional transducer. Gain accounts for losses referred to a point on the electrical side of the transducer.
Pulse duration	τ	s	The duration of a signal pulse.
Effective pulse duration	τ_{eff}	s	The duration of a square-shaped pulse that has the same energy as the echosounder-pulse shape after reception processing.
Equivalent two-way beam angle	Ψ	dB re 1 sr	The solid angle subtended by an ideal conical beam that would produce the same volume integral as the square of the normalized transducer directivity.
S_a correction factor	$S_{a\,\text{corr}}$	dB re 1	A correction factor to account for differences between the τ used to calculate S_V and τ_{eff}.
Region thickness	T	m	The thickness, or height, of a defined region.
Mean S_V	$S_{V\,\text{mean}}$	dB re 1 m^2 m^{-3}	The mean S_V of samples within a defined region of thickness, T.

Introduction

The Summer 2018 Survey of the California Current Ecosystem (CCES), conducted by the Southwest Fisheries Science Center (SWFSC), was augmented by five Saildrones, each outfitted with a miniature wide-bandwidth transceiver (Simrad WBT Mini) configured with a dual-frequency transducer (Simrad ES38-18/200-18C). The Saildrones were assessed for their potential to enhance ship-based surveys and research. To optimize the accuracy and precision of the Saildrone-based data collections, each of the five WBT Mini and transducer pairs were calibrated. The 38-kHz three-sector split-beam channel and the 200-kHz single-beam channel were calibrated in both narrowband (CW) and wideband (FM) modes. This report describes the system characterization, calibration methods and results, and issues encountered. This report

also includes recommendations for software and hardware development, and refinements to calibration procedures.

Methods

Calibration Apparatus

Calibrations of the WBT Mini systems were conducted in the SWFSC Technology Tank (Demer et al. 2015) prior to the survey, 22 - 25 May 2018. Three of the echosounder systems were also calibrated following the survey, two in October and November 2018 and one in January 2019. The Technology Tank is 10-m deep by 10-m wide by 20-m long. The 2 million liters of water in the tank can emulate a variety of seawater conditions, e.g., with user adjustable salinity (freshwater to ~35 PSU) and temperature (~2 to 30°C). For these calibrations, the tank water temperature was ~20°C and the salinity was ~33.3 PSU.

In succession, each of the five transducers was mounted on the pitch tray of a rotate-pitch pole (**Fig. 1**) installed in the center of a bridge located approximately 6 m from the western end of the tank. This apparatus positioned the transducer ~0.5 to 2 m below the water surface. Two stepping motors enabled remote control of the transducer rotation and pitch. The transducer was oriented to transmit acoustic pulses vertically toward the tank floor, i.e., pitch ~0°.
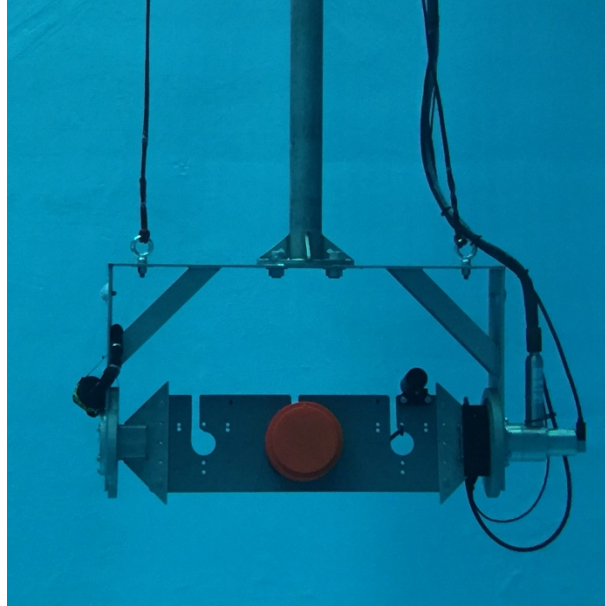

Figure 1. The rotate-pitch pole with an ES70-18CD transducer (not used in this study) installed in the Technology Tank at the SWFSC. A stepping motor (right side) enabled remote control of transducer pitch. A second stepping motor located on the top of the vertical pole (not shown) was used to remotely adjust the transducer rotation. An inclinometer on the pitch tray (black cylinder mounted on transducer bracket) was used to independently measure pitch angles.

Impedance

To ensure the transducers were functioning correctly, electrical impedance (Z_{et}; Ω) was measured for the three sectors of the ES38-18 and the single element of the 200-18C using an impedance analyzer (Agilent 42964A). Before the measurements, the impedance analyzer was configured with open and short fixture compensations to eliminate effects of the measurement-cable impedance. The impedance measurements are for the transducer, its molded 2-m cable, and the 3-m extension cable used during the survey.

Measurements of Z_{et} were made with the transducers in water, using 801 samples, 2-kHz bandwidth, 5-V oscillator level, and 5-sweep averages. The sweep frequencies were 32-47 kHz for the ES38-18 and 142-285 kHz for the 200-18C, selected to obtain complete admittance circles.

The impedance magnitude ($|z_{et}|$; Ω), conductance (G ; S), and phase (φ; °) of the five transducers were compared. The usable bandwidths for each transducer were estimated using frequencies for which $|z_{et}| > 50Ω$ and $|\varphi| < 45°$ (personal communication, Lars Andersen, March 2016).

Linear Transmit Power

If the power input to a transducer is too high, either cavitation bubbles may form on or in front of the transducer, or the sinusoidal waveform may be distorted. The latter results in the transfer of energy from the fundamental frequency to higher-frequency harmonics. Both cases cause the output power to change non-linearly versus input power. To avoid these effects, transmit powers should be less than or equal to the values recommended for common transducers (Korneliussen et al., 2008; Demer et al., 2017), depending on their operating frequency and beamwidth. Presently, however, there are no recommendations for maximum transmit powers for 18⁰-beamwidth, 38- or 200-kHz transducers.

Measurements were made of the maximum linear transmit powers for the ES38-18/200-18C transducer (SN 101), installed on the rotate-pitch pole, positioned ~1 m below the water surface, and oriented to project at a 45° angle downward and toward the east-end of the tank. A hydrophone (Reson TC4034-1; SN 4216111) was suspended in the tank and positioned approximately on the axis of the 38-kHz transducer beam at a range of ~4.5 m. The hydrophone was connected to a pre-amplifier (Stanford Research SR560) using AC coupling; 50 Ω output; 6 dB, 10- and 300-kHz bandpass-filter cutoff frequencies; low-noise 20-dB gain; and line power. The output of the amplifier was connected to a digital acquisition device (DAQ; National Instruments NI-9223), controlled with software (PAMGuard V1.15.09), and configured with a 1-MHz sampling rate.

With the transducer connected to a WBT Mini (SN 264024), the Simrad EK Mission Planner software (V3.2.1) uploaded mission plans to transmit narrowband, continuous-wave (CW) and wideband, frequency-modulated (FM) pulses with 1.024-ms pulse durations, 1-s transmit

intervals, and 100- to 500-W transmit powers. For each pulse type and transmit power, waveforms of ~10-s duration were recorded. After obtaining the 38-kHz measurements, the hydrophone was relocated 1.8° forward of the ES38-18, which, at a range of 4.8 m, placed it approximately on-axis of the 200-18C beam. Similar measurements were then repeated for the 200-kHz transducer using transmit powers ranging from 50 to 250 W.

For both frequencies, recordings of CW pulses for each transmit power were loaded into analysis software (Matlab, The Mathworks, Inc.). The ~10 transmit pulses within the recordings were isolated and their power spectral densities (PSD) were computed using Welch's method, a Hamming window, 50% overlap, and a 4,096-point fast Fourier transform (FFT). The means of the maximum PSDs for each pulse were plotted versus transmit power.

To verify results from the hydrophone measurements for the 200-kHz transducer, additional measurements were conducted by first setting the transducer pitch to 0° (vertically downward). A 38.1-mm diameter sphere (AST #5) made from tungsten-carbide with 6% cobalt binder material (WC) was then positioned below the transducer at a range of 5.7 m and 1.5º forward of the ES38-18, placing it approximately on-axis of the 200-18C. Using EK Mission Planner, the WBT Mini was programmed to transmit CW pulses with powers ranging from 200 to 250 W. Target strengths (TS; dB re 1 m^2) of the sphere were then compared versus transmit power.

Sphere Calibration

The standard sphere method (Foote et al., 1987; Demer et al., 2015) was used to calibrate the WBT Mini systems in both CW and FM modes. The 38.1-mm diameter WC sphere (AST #5) was suspended below the transducer using three remotely controlled, motorized downriggers. Triangulated downriggers were positioned such that two downriggers were located on the west side of the west gantry and one on the west side of the east gantry. The sphere was positioned at ~4-m range to avoid sidelobe reflections at larger ranges.

System calibrations were performed using the settings used during the Saildrone survey. However, because the calibration program in the EK Mission Planner software does not allow simultaneous transmit pulses at 38 and 200 kHz, each WBT Mini was first set to EK80 Mode and operated using EK80 software. This step provided information about the downrigger-line lengths needed to move the sphere throughout the 38- and 200-kHz beams. Then, the WBT Mini was setup using the EK Mission Planner software and the parameters in **Table 1.**

Table 1: Calibration and survey parameters for the 38- and 200-kHz WBT Mini systems

-	38 kHz	200 kHz
Transmit Power (W)	500	215
Pulse Duration (µs)	1024	1024
FM Bandwidth (kHz)	34 - 45	190 - 230
Range (m)	20	20
Ramping	Fast	Fast

Next, a mission plan was uploaded to the WBT Mini, activated, and the sphere was moved throughout the 38- and 200-kHz beams.

There were few single-target detections at some angular positions within the acoustic beam. The number and locations of detections were modulated by the transducer rotation. This may be due to reduced phase coherence resulting from sidelobe or back-radiation reflections. To mitigate this, the sphere was moved throughout the beam for rotations of ~0°, 45°, and 90°. The single-target detections from each rotation were combined to map the full beam pattern. Next, the mission plan was halted, the WBT Mini was put into sleep mode, and the raw data was retrieved from the internal USB drive, archived, and processed to obtain calibration results.

Angle Sensitivity

For TS measurements made with the split-beam ES38-18 transducer, single-target positions are estimated by converting the electrical phase angles for signals received by the three sectors ($\theta_{e\alpha}$ and $\theta_{e\beta}$; electrical°) to mechanical angles (α and β; geometric°) using angle sensitivities (Λ_α and Λ_β; electrical°/geometric°) for the orthogonal alongships and athwartships planes, respectively (Demer et al., 1999):

$$\frac{\pi}{180}\theta_{e\alpha} = \Lambda_\alpha \sin(\alpha); \frac{\pi}{180}\theta_{e\beta} = \Lambda_\beta \sin(\beta). \tag{1}$$

Due to the narrow beamwidth of the ES38-18/200-18C, the small-angle approximation yields $\sin(\alpha) = \frac{\pi}{180}\alpha$, allowing Eq. 1 to be simplified and rearranged:

$$\alpha = \frac{\theta_{e\alpha}}{\Lambda_\alpha}; \beta = \frac{\theta_{e\beta}}{\Lambda_\beta}. \tag{2}$$

Typically, the default values for Λ_α and Λ_β are used, as defined in the software. If Λ_α and Λ_β are incorrect ($\Lambda_{\alpha\text{bad}}$ and $\Lambda_{\beta\text{bad}}$), then the estimated α and β, and the derived beamwidths ($\alpha_{-3\text{ dB}}$ and $\beta_{-3\text{ dB}}$; °), are inaccurate:

$$\alpha_{\text{bad}} = \sin^{-1}\left(\frac{\theta_{e\alpha}}{\Lambda_{\alpha\text{bad}}}\right); \beta_{bad} = \sin^{-1}\left(\frac{\theta_{e\beta}}{\Lambda_{\beta\text{bad}}}\right) \tag{3}$$

If, after calibration, the Λ_α and Λ_β and estimated $\alpha_{-3\text{ dB}}$ and $\beta_{-3\text{ dB}}$ are not updated in the WBT Mini settings, then the split-beam measurements of TS are correctly compensated for beam directivity, despite incorrect estimates of α and β. However, if the Λ_α and Λ_β, α and β, and $\alpha_{-3\text{ dB}}$ and $\beta_{-3\text{ dB}}$ are correct for the split-beam 38-kHz channel, they may be used to accurately estimate the sphere TS, α and β, and $\alpha_{-3\text{ dB}}$ and $\beta_{-3\text{ dB}}$ for the single-beam 200-kHz channel. Accurate Λ_α and Λ_β may be derived using accurate and independent measurements of α and β within the 38-kHz beam:

$$\Lambda_\alpha = \Lambda_{\alpha\,bad}\,\frac{\alpha_{bad}}{\alpha}, \; \Lambda_\beta = \Lambda_{\beta\,bad}\,\frac{\beta_{bad}}{\beta}. \tag{4}$$

Alternatively, accurate Λ_α and Λ_β may be derived from inaccurate measurements of $\alpha_{-3\,\text{dB}}$ ($\alpha_{-3\,\text{dB}\,bad}$) and $\beta_{-3\,\text{dB}}$ ($\beta_{-3\,\text{dB}\,bad}$) – obtained using $\Lambda_{\alpha\,\text{bad}}$ and $\Lambda_{\beta\,\text{bad}}$ – and independent, accurate measurements of $\alpha_{-3\,\text{dB}}$ and $\beta_{-3\,\text{dB}}$:

$$\Lambda_\alpha = \Lambda_{\alpha\,\text{bad}}\,\frac{\alpha_{-3\,\text{dB}\,bad}}{\alpha_{-3\,\text{dB}}}; \; \Lambda_\beta = \Lambda_{\beta\,\text{bad}}\,\frac{\beta_{-3\,\text{dB}\,bad}}{\beta_{-3\,\text{dB}}}. \tag{5}$$

To accurately estimate the 38-kHz Λ_α and Λ_β, an ES38-18/200-18C transducer (SN 105) was installed on the rotate-pitch pole, positioned ~1 m below the water surface, and oriented to project vertically toward the tank floor. The sphere was placed on the axis of the 38-kHz transducer at a range of 3.7 m. The WBT Mini (SN 264032) was put into EK80 mode and controlled using the EK80 software (V 1.12.1). Without moving the sphere, the transducer pitch was modulated from ~-9° to 9° in 1° increments, effectively moving the sphere across the alongships plane of the transducer beam. For each increment, raw data was recorded for CW and FM modes, and the pitch positions were recorded from an inclinometer (PNI Sensor Corporation TCM5.0) on the pitch tray.

An estimate of accurate Λ_α was derived with inclinometer measurements of α and EK80-derived values of α_{bad}. For comparison, accurate Λ_α was also derived using Eq. 5 solved with an estimate of $\alpha_{-3\,\text{dB}}$ [from the Simrad beam model fit to the EK80-derived beam-uncompensated TS versus the corresponding pitch angles from the inclinometer (α)], and an estimate of $\alpha_{-3\,\text{dB}\,bad}$ derived from the EK80 calibration software.

Transducer Separation

The conversion of 38-kHz split-beam positions to positions in the 200-kHz beam involves the slant angles from the axis of the 38-kHz transducer to the target in the alongships (α_{38}) and athwartships planes (β_{38}), the ranges from the 38- and 200-kHz transducers to the target ($r_{38,200}$; m), and the effective alongships distance between the 38- and 200-kHz transducers (d_α; m) (Demer et al., 1999):

$$\alpha_{200} = \sin^{-1}\left(\frac{r_{38}\cdot\sin(\alpha_{38})-d_\alpha}{r_{200}}\right); \; \beta_{200} = \sin^{-1}\left(\frac{r_{38}\cdot\sin(\beta_{38})}{r_{200}}\right). \tag{6}$$

For the ES38-18/200-18C transducer, the separation in the athwartships plane, d_β, is assumed to be 0 m. However, an accurate estimate of d_α is necessary to accurately map the 200-kHz beam pattern, and estimate the transducer $\alpha_{-3\,\text{dB}}$ and $\beta_{-3\,\text{dB}}$ and offset angles (α_0 and β_0; °) in the alongships and athwartships planes, respectively.

Calibration data from the WBT Mini (SN 264032) with independently measured Λ_α and $\alpha_{-3\,\mathrm{dB}}$ and $\beta_{-3\,\mathrm{dB}}$ were loaded into Echoview. An ECS file was created and edited to set the 38-kHz transducer Λ_α and Λ_β to 9.33 electrical°/geometric° and the G_0, $\alpha_{-3\,\mathrm{dB}}$ and $\beta_{-3\,\mathrm{dB}}$, and α_0 and β_0 to those derived from the calibration of that echosounder and transducer (**Table 3**). Single-target detection operators were then used (**Table 2**) to detect single-target TS data, which were exported to CSV files. In Matlab, a nonlinear least-squares regression with a bi-square weight function was used to find the optimal d_α, used for converting α_{38} and β_{38} to α_{200} and β_{200} (Eq. 6), to minimize the error between the 200-kHz beam-uncompensated TS to the Simrad beam model.

Calibration Processing

Gain, Beamwidths, and Offset Angles

The five systems were calibrated prior to the survey, from 22 to 25 May 2018. Following the survey, in October and November 2018, two of the systems (WBT-Minis 264025 and 264026) were re-calibrated with and without biofouling on the transducers, which accumulated during the survey. In January 2019, a third system (WBT-Mini 264032) was re-calibrated with the transducer cleaned of biofouling. A calibration with biofouling on the transducer was not possible as the transducer was cleaned prior to arriving at SWFSC. For each WBT Mini / transducer pair, the raw data was loaded into Echoview (V 9.0.323.34916) and an Echoview Calibration Supplement (ECS) file was created to apply the more accurate estimates of Λ_α and Λ_β to the 38-kHz transducer. Single-target detection parameters (Echoview Method 2; **Table 2**) were then used to obtain TS measurements of the sphere from both the 38-kHz split-beam and 200-kHz single-beam data. Because the 38-kHz target positions were used to derive 200-kHz target positions, only those data that contained both 38- and 200-kHz target detections were retained. The single-target TS data for both frequencies were then exported to CSV files.

Table 2: Single-target detection parameters (Echoview)

-	38 kHz	200 kHz
Single-Target Detection Method	Split-beam Method 2	Single-beam Method 2
Beam-compensated TS threshold	-50.00	-50.00
Pulse-length determination level	6.00	6.00
Minimum normalized-pulse length	0.40	0.60
Maximum normalized-pulse length	1.50	1.50
Beam-compensation model	Simrad	N/A
Maximum beam compensation	6.00	N/A
Maximum standard deviation of alongships/athwartships-axis angles	0.60 / 0.60	N/A

To derive calibrated estimates of $\alpha_{-3\,\text{dB}}$ and $\beta_{-3\,\text{dB}}$, and α_0 and β_0, the 38-kHz single-target CSV files were loaded into Matlab and the target positions and beam-uncompensated TS were fit to the Simrad beam model (see Demer et al., 1999) using a nonlinear least-squares regression with a bi-square robust-weight function. The on-axis TS ($TS_{\text{on-axis}}$; dB re 1 m^2) was calculated using the mean beam-compensated TS for targets having a beam compensation < 0.1 dB. The calibrated transducer gain (G_0; dB re 1) was then derived by compensating the pre-calibrated gain ($G_{0\,\text{old}}$; dB re 1), used to obtain the beam-uncompensated TS values, by half the difference between $TS_{\text{on-axis}}$ and the theoretical TS (TS_{theory}; dB re 1 m^2) of the 38.1-mm diameter WC sphere:

$$G_0 = G_{0\,\text{old}} + \frac{TS_{\text{on-axis}} - TS_{\text{theory}}}{2} \ . \tag{7}$$

The 38-kHz target positions, adjusted by the calibrated α_0 and β_0, were then converted to 200-kHz target positions using r_{38}, r_{200}, and the estimated d_α (Eq. 6). The derived 200-kHz target positions and beam-uncompensated TS were then similarly fit to the Simrad beam model to derive calibrated estimates of $TS_{\text{on-axis}}$, $\alpha_{-3\,\text{dB}}$ and $\beta_{-3\,\text{dB}}$, and α_0 and β_0. $TS_{\text{on-axis}}$, in conjunction with TS_{theory} and $G_{0\,\text{old}}$, were then used to obtain the calibrated 200-kHz G_0 (Eq. 7).

Equivalent Two-Way Beam Angle

When computing volume backscatter (S_V; dB re 1 m^2 m^{-3}), the sampling volume is a function of the range, pulse duration (τ; s), and equivalent two-way beam angle (Ψ; dB re 1 sr). Values of Ψ are typically taken from the manufacturer-supplied transducer specification because accurate measurements of Ψ require independent measurement of target positions (Demer et al., 2015). Otherwise, inaccurate Λ_α and Λ_β will result in inaccurate estimates of $\alpha_{-3\,\text{dB}}$ and $\beta_{-3\,\text{dB}}$ and Ψ. However, using accurate 38-kHz Λ_α and Λ_β, Ψ may be accurately estimated from measurements of $\alpha_{-3\,\text{dB}}$ and $\beta_{-3\,\text{dB}}$ (Urick, 1983):

$$\Psi = 10\log_{10}\left(\frac{\alpha_{-3\,\text{dB}} \cdot \beta_{-3\,\text{dB}}}{5800}\right). \tag{8}$$

S_a Correction

The sampling volume, used to derive S_V, is a function of Ψ, r, and the effective pulse duration (τ_{eff}; s). Accurate estimates of τ_{eff} are derived from the EK80-WBT Mini parameters and filter coefficients that define the transmitted pulse shape. Any residual differences between the theoretical and actual pulse shapes are taken into account by a correction factor ($S_{a\,\text{corr}}$; dB re 1). Estimates of $S_{a\,\text{corr}}$ were obtained using τ_{eff} derived in Echoview (**Table 3**). $S_{a\,\text{corr}}$ was calculated using an algorithm described by Echoview. First, the mean S_V ($S_{V\,\text{mean}}$; dB re 1 m^2 m^{-3}) was calculated for a region of thickness (T; m) surrounding the sphere echo when it was measured near or on the axis of the acoustic beam. The theoretical S_V of the sphere ($S_{V\,\text{theory}}$; dB re 1 m^2 m^{-3}) was then calculated from TS_{theory}, T, Ψ, and r:

$$S_{V_\text{theory}} = TS_\text{theory} - 20\log_{10}(r) - 10\log_{10}(T) - \Psi. \tag{9}$$

The pre-calibrated S_{a_corr} ($S_{a_\text{corr}_\text{old}}$; dB re 1) was then compensated by the difference between S_{V_mean} and S_{V_theory} to obtain the calibrated S_{a_corr}:

$$S_{a_\text{corr}} = S_{a_\text{corr}_\text{old}} + \frac{S_{V_\text{mean}} - S_{V_\text{theory}}}{2}. \tag{10}$$

In Echoview, the ECS-file was updated to apply the calibrated 38- and 200-kHz G_0, $\alpha_{-3\text{ dB}}$ and $\beta_{-3\text{ dB}}$, α_0 and β_0, and Ψ. For the 38-kHz system, only transmissions with the calibration sphere on-axis were retained by restricting the maximum beam compensation parameter in the single-target detection variable to 0.1 dB. A region was created around the sphere echo, then values of TS and S_V from that region were exported to CSV-files. For each transmission, values of S_{V_mean} and T, derived from the S_V data, and r, derived from the TS data, were obtained. Those parameters, in conjunction with S_{V_theory}, were used to calculate S_{a_corr} for each transmission, which were averaged across all transmissions to obtain the calibrated S_{a_corr} using Eq. 10.

For the 200-kHz transducer, the target positions were first calculated in Matlab by compensating the 38-kHz target positions by the transducer d_α and the r for both transducers (Eq. 6). The beam compensation for each target was then calculated using the calibrated 200-kHz $\alpha_{-3\text{ dB}}$ and $\beta_{-3\text{ dB}}$, and α_0 and β_0. To obtain near-axis S_V-sphere echoes, a CSV file, formatted in the Echoview S_V-CSV-file specification, was then created such that target positions requiring <0.1 dB compensation contained a valid sample, otherwise no samples were defined. In Echoview, this CSV file was loaded, then the resulting S_V variable was reduced (via the Reduced Pings operator) such that data remained only during times when the target was near or on the axis of the 200-kHz transducer. The 200-kHz data was then matched to those times (via the Matched Ping Times operator) such that only near-axis TS and S_V data remained. Similar to the 38-kHz echogram, a region was created around the sphere echo. For data within this region, the values of TS and S_V were exported to obtain values of S_{V_mean}, T, and r for each transmission. Those parameters, in conjunction with S_{V_theory}, were used to obtain the mean calibrated S_{a_corr} using Eq. 10.

FM Mode

Standard sphere calibrations were also performed while sequentially transmitting wideband FM pulses from the 38- and 200-kHz transducers (**Table 1**). The resulting 38-kHz raw data was replayed in the EK80 software (V 1.12.2), and the EK80 calibration utility was used to obtain the calibrated G_0, $\alpha_{-3\text{ dB}}$ and $\beta_{-3\text{ dB}}$, and α_0 and β_0. Currently, neither EK80 nor Echoview software utilize $S_{a\text{ corr}}$ for FM data.

To account for changes between the default Λ_α and Λ_β used by the EK80 calibration utility and those derived from independent measurements, the resulting $\alpha_{-3\text{ dB}}$ and $\beta_{-3\text{ dB}}$, and α_0 and β_0

were compensated (Eq. 5). The Λ_α measured independently from the CW data is valid at 38 kHz, but can be compensated as a function of frequency (Bodholdt, 2002):

$$\Lambda_\alpha = \frac{2\pi f d}{c} = \frac{2\pi f' d}{c} \cdot \frac{f}{f'} = \Lambda_\alpha' \cdot \frac{f}{f'},$$ (11)

where f' is 38 kHz and Λ_α' the derived alongship angle sensitivity at 38 kHz. Likewise, the transducer G_0 and $\alpha_{-3\,\text{dB}}$ and $\beta_{-3\,\text{dB}}$ can also be compensated as a function of frequency:

$$g_0 = \frac{\eta 4\pi A f^2}{c^2} = \frac{\eta 4\pi A f'^2}{c^2} \cdot \frac{f^2}{f'^2} = g_0' \cdot \frac{f^2}{f'^2}$$ (12)

$$\alpha_{-3\,\text{dB}} = \frac{c}{Df} = \frac{c}{Df'} \cdot \frac{f'}{f} = \alpha_{-3\,\text{dB}}' \cdot \frac{f'}{f}; \quad \beta_{-3\,\text{dB}} = \frac{c}{Df} = \frac{c}{Df'} \cdot \frac{f'}{f} = \beta_{-3\,\text{dB}}' \cdot \frac{f'}{f},$$ (13)

where g_0 is the linear gain ($g_0 = 10^{G_0/10}$). FM data from the single-beam 200-kHz transducer cannot be calibrated in the EK80 software. Single target detections can be performed in Echoview, but TS spectra from all single targets cannot be exported.

Results

Impedance

Corresponding to frequencies where $|z_{et}| > 50\Omega$ and $|\varphi| < 45°$, the usable bandwidths for the ES38-18 and ES200-18C transducers are 33-46 kHz and 179-232 kHz, respectively. The measured $|z_{et}|$, G, and φ are plotted over the usable bandwidth for each of the five transducers (**Fig. 2**). For the ES38-18, the means and ±2 standard deviations (95% confidence intervals) are shown for the measurements of the three sectors.
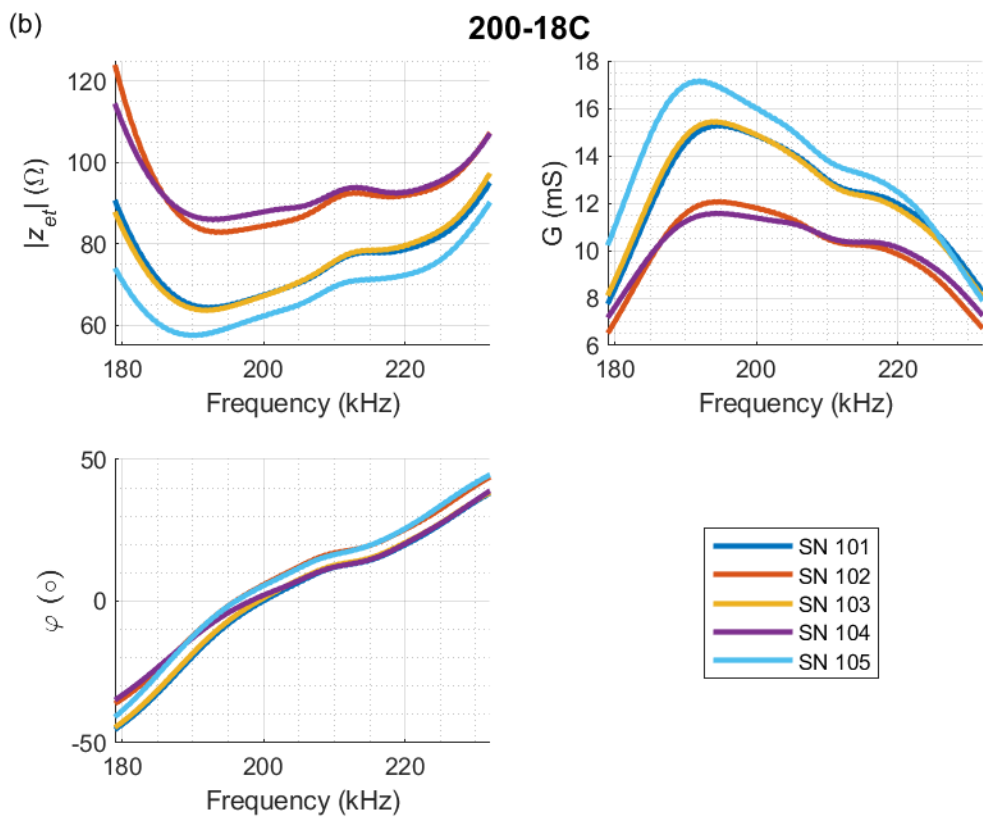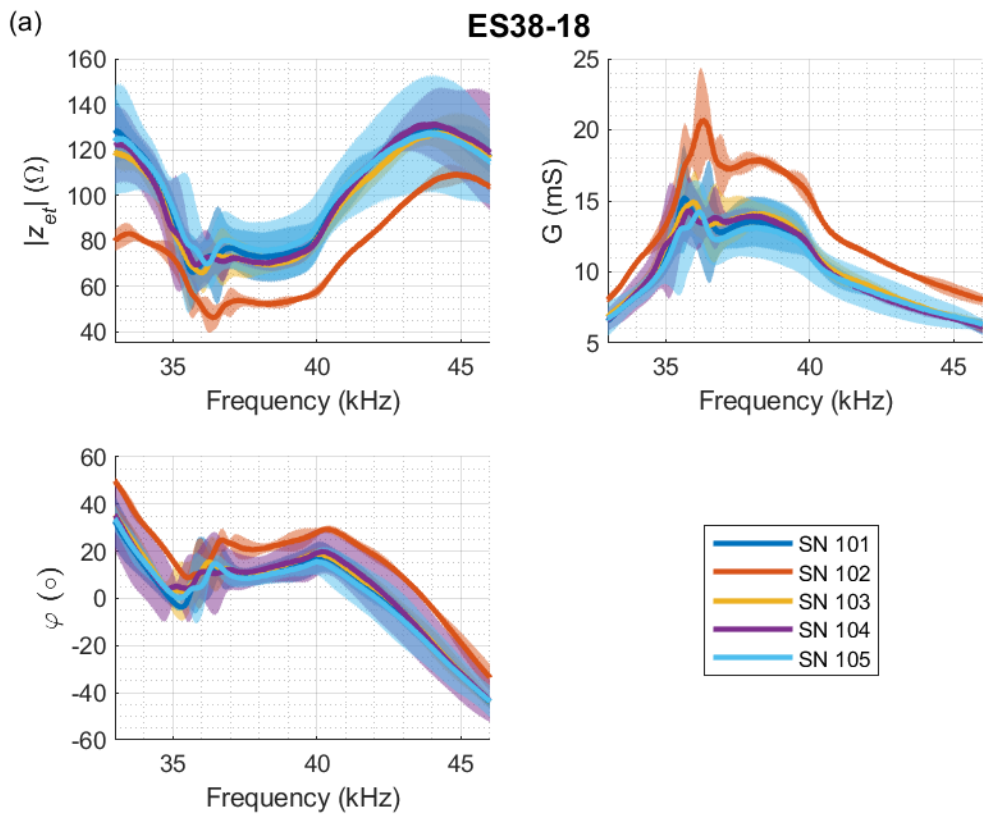
(a) **ES38-18**

(b) **200-18C**

Figure 2. Impedance magnitude ($|z_{et}|$), conductance (G), and phase (φ) versus frequency for the five ES38-18/200-18C transducers. Data are plotted over the usable bandwidth derived from measurements of $|z_{et}|$ and φ. The ES38-18 measurements (a) are averaged over the three transducer sectors, with 95% confidence intervals calculated using ±2 standard deviations. The 200-18C measurements (b) are for the single transducer element.

The ES38-18 impedances indicate that transducer SN 102 has consistently lower $|z_{et}|$, ~18 Ω less at 38 kHz, and higher G versus frequency, compared to the other transducers which have similar impedance characteristics. The 200-18C impedances indicate that transducers SN 102 and SN 104 are different from the other three, with $|z_{et}|$ values ~20 Ω higher at 200 kHz.

Linear Transmit Power

The maximum linear transmit powers were measured for one WBT Mini / ES38-18/200-18C system. For each transmit power, the transmit pulses in the recording were isolated and their PSDs computed (**Fig. 3**).
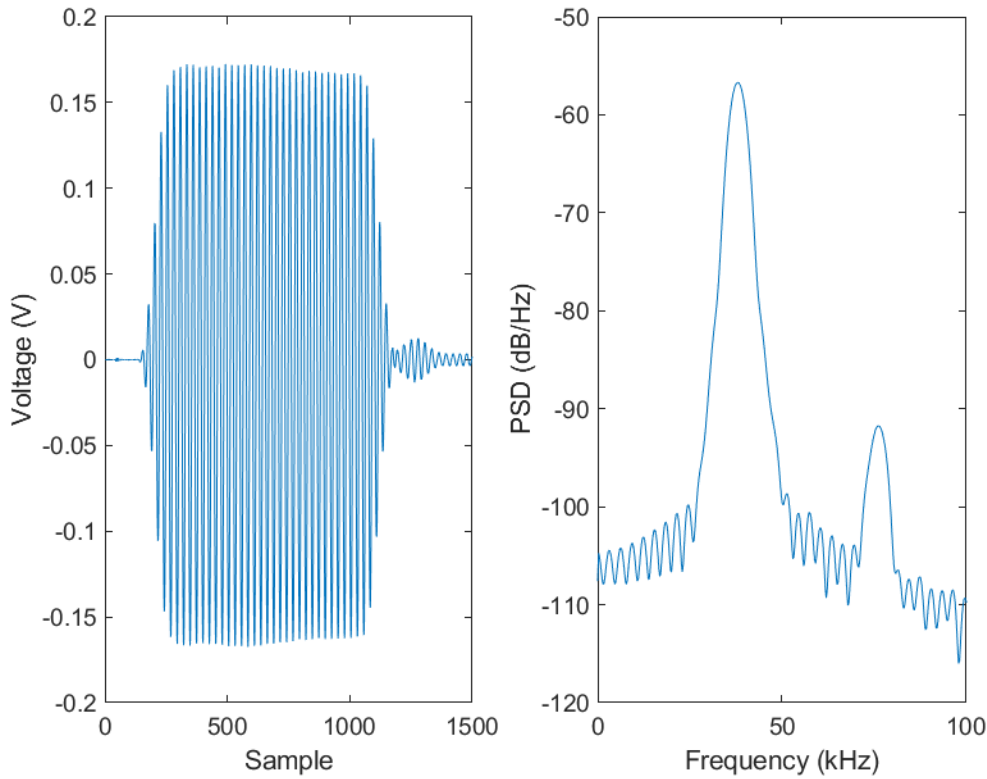

Figure 3. Received transmit pulse and corresponding PSD for the ES38-18 operating with a 100-W transmit power.

For each transmit power, the maximum PSDs of all transmit pulses were averaged. The mean of the maximum PSDs were then compared across transmit powers (**Fig. 4**).
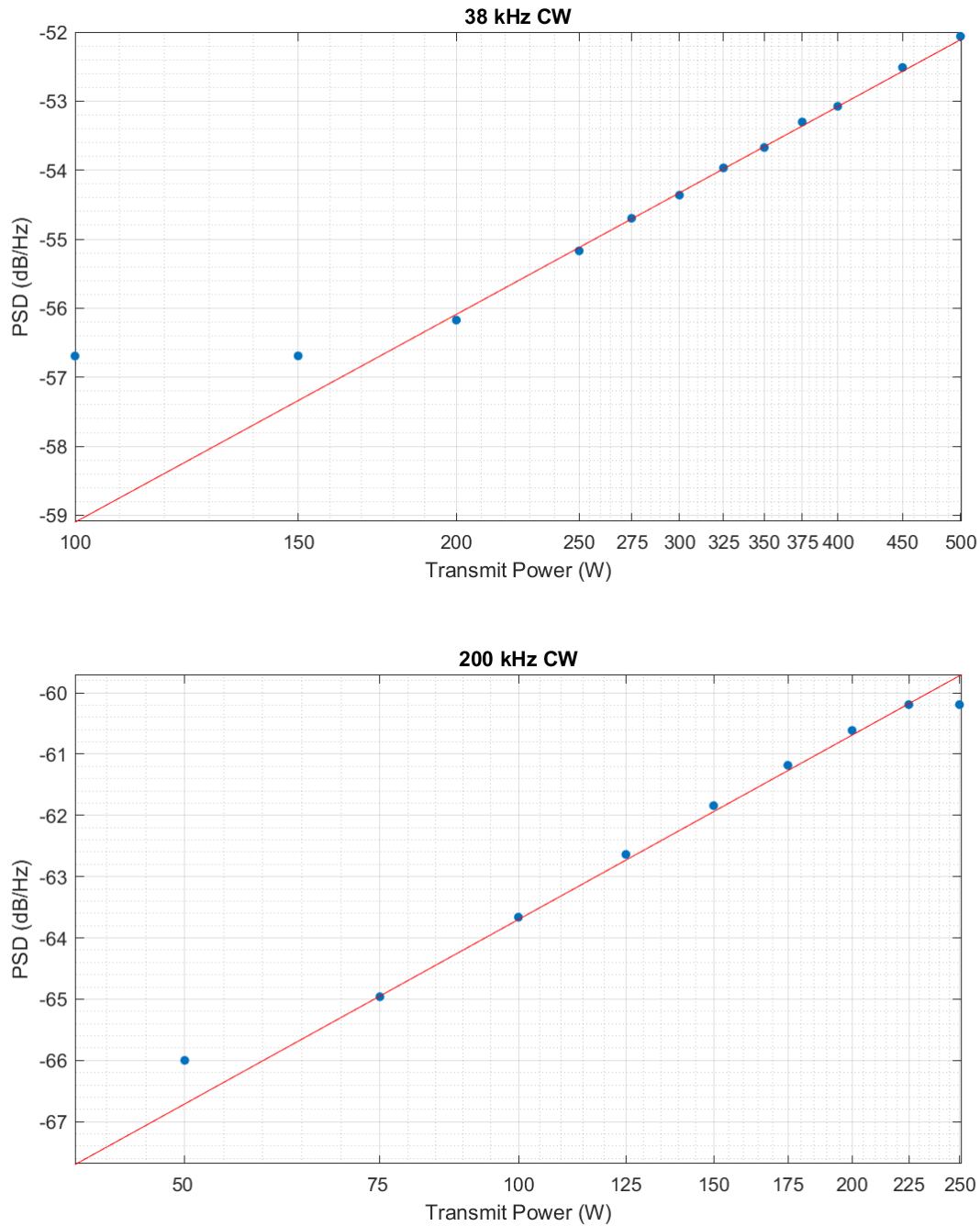
Figure 4. Average maximum PSD versus transmit power for the ES38-18 and 200-18C transducers (blue points). When operating in the linear range, indicated by the 1:1 line (solid red), changes in the transmit power result in proportional changes in the PSD.

The ES38-18 has a linear response between ~200 and 500 W, the maximum allowable transmit power. The PSD does not decrease proportionally below 200 W, which indicates that the transceiver does not decrease the output power according to the setting.

The 200-18C has a linear response between ~75 and 225 W, but the PSD does not increase for greater transmit power. Similar to the ES38-18, decreases in transmit power below ~75 W do not proportionally reduce the PSD.

To verify the maximum linear transmit power of the 200-18C, on-axis measures of sphere TS were obtained using transmit powers from 200 to 250 W, with the resulting power levels recorded and compared (**Fig. 5**).
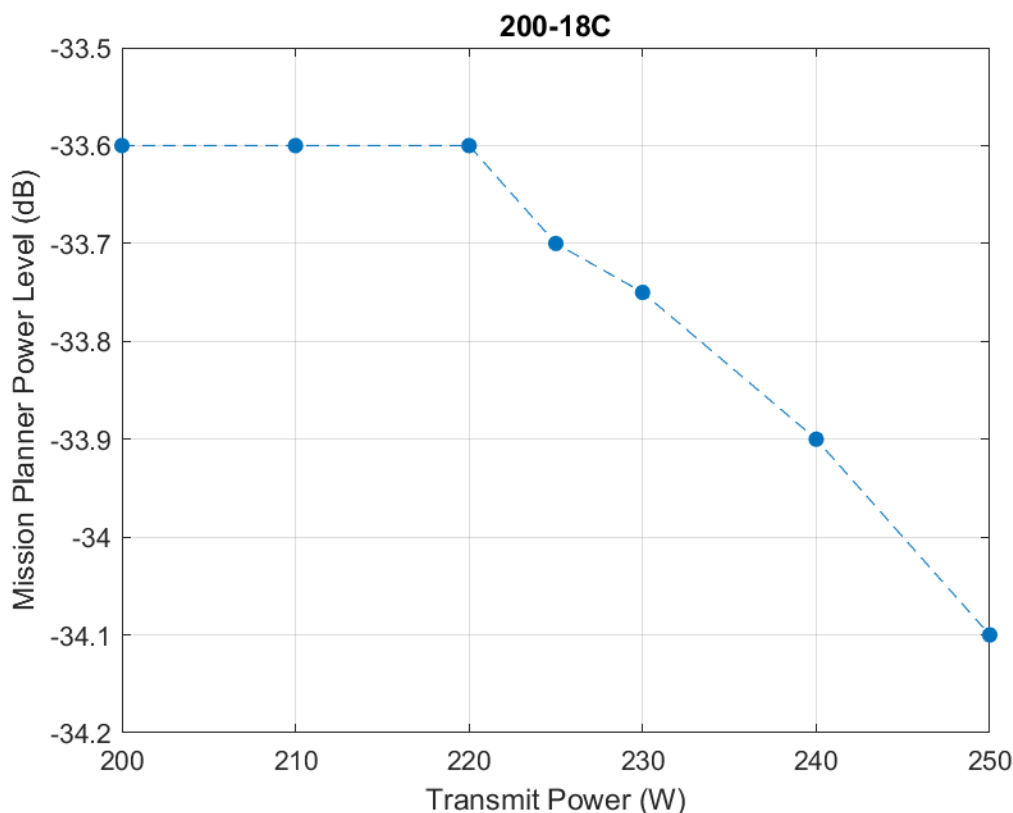

Figure 5. Power level versus transmit power for single-target detections of a 38.1-mm WC sphere from the EK Mission Planner calibration utility for a 200-18C transducer. Changes in the transmit power above 220 W result in changes in the received sphere power level, indicating the transmitted power is not being accurately defined when deriving sphere echo levels.

The single-target power levels reported by the EK Mission Planner calibration program indicate a flat response from the sphere up to a 220-W transmit power. Above this value, the power level decreases with increasing transmit power. Additionally, the WBT Mini transceiver has a maximum transmit power of 250 W per channel for a 55 Ω load. Because the 200-18C is a single-element transducer with a measured impedance of ~66 Ω, the maximum transmit power achievable by the WBT Mini is ~208 W. According to Simrad (personal communication, June 2018), the power limits are conservative values.

With the 200-kHz measurements indicating a maximum linear transmit power between 225 and 250 W (hydrophone), and 220 and 225 W (sphere *TS*), a transmit power of 215 W for the 200-

18C is conservative. Because the 38-kHz measurements did not indicate non-linear effects for the maximum transmit power, 500 W is conservative for the ES38-18. Although these measurements were made for only one transducer, these conservative maximum linear transmit powers were assumed for the other ES38-18/ES200-18 transducers.

Angle Sensitivity

TS measurements of a 38.1-mm diameter WC sphere were collected for various transducer-pitch angles as measured independently by an inclinometer. For each pitch angle, values of the beam-uncompensated TS and target positions were obtained using the EK80 software (V 1.12.2). The estimates of α from the inclinometer, α_{bad} from the EK80, and the default 38-kHz $\Lambda_{\alpha_{\mathrm{bad}}}$ (10.5 electrical°/geometric°), were used to estimate the true Λ_α (Eq. 4; **Fig. 6**).
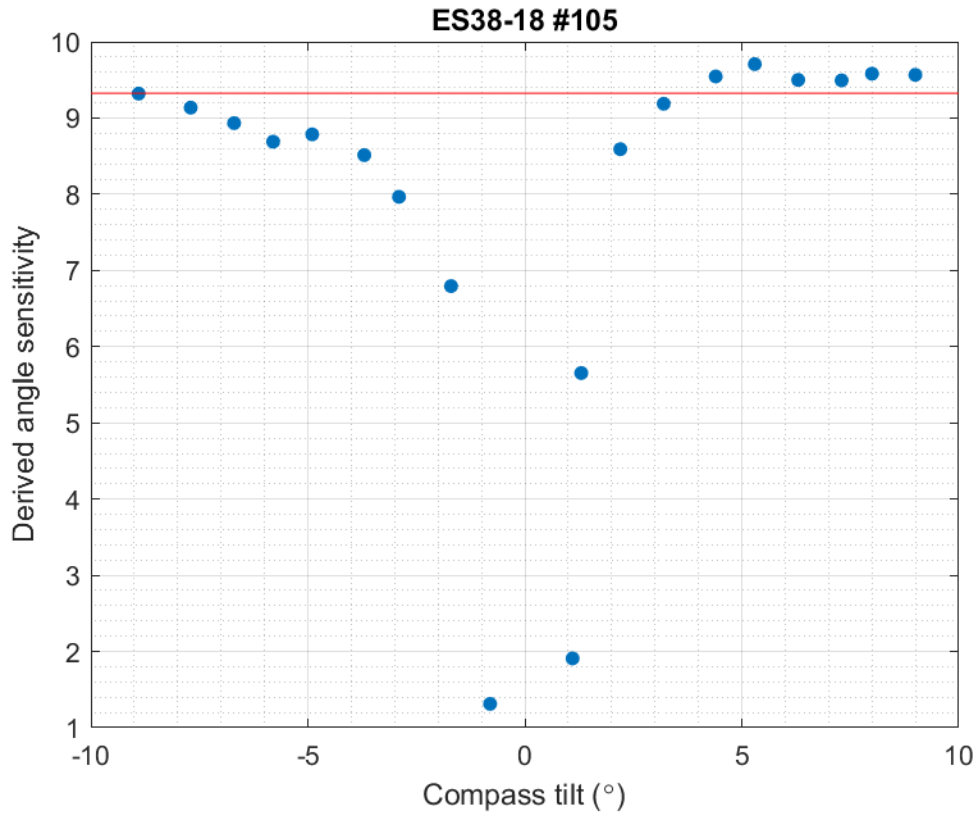

Figure 6. Estimates of true alongships angle sensitivity at various transducer pitch angles, derived using independent measures of the transducer pitch (i.e., target position) and target positions from the EK80 software using the default alongships angle sensitivity. The horizontal red line indicates the mean angle sensitivity for pitch angles greater or less than 5 and -5⁰, respectively.

When the sphere is close to the beam axis of the 38-kHz transducer, small differences between α and α_{bad} can lead to large changes in Λ_α. To eliminate this sensitivity of near-axis measurements, the Λ_α was calculated using the mean of angle sensitivities for pitch angles > 5⁰ or < -5⁰. This resulted in a 38-kHz Λ_α of 9.33 electrical°/geometric°, 11% lower than the default Λ_α of 10.5 electrical°/geometric° (**Fig. 6**)

16

Alternatively, the beam-uncompensated TS measurements and true target positions from the inclinometer were fitted to the Simrad beam model, resulting in an estimated 38-kHz $\alpha_{-3\text{ dB}}$ of 16.94° (**Fig. 7**).
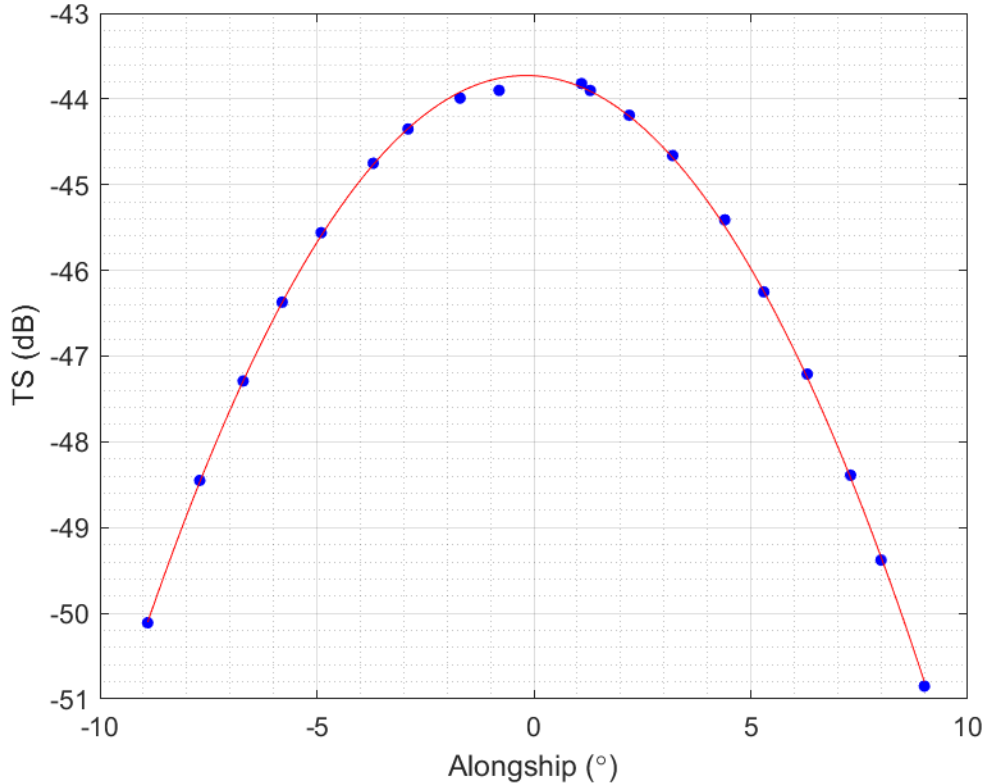

Figure 7. Beam-uncompensated TS (blue dots) in the alongships plane fitted to the Simrad beam model (red line).

Using the measurements of TS versus sphere position from the calibration of the same WBT Mini / transducer pair, the EK80 calibration utility estimated the 38-kHz $\alpha_{-3\text{ dB}}$ = 15.06°, using the default Λ_α of 10.5 electrical°/geometric°. From Eq. 5, the true Λ_α was estimated to be 9.33 electrical°/geometric°, matching exactly the Λ_α derived from the comparison of EK80-derived and independently measured target positions.

The specification sheet supplied by Simrad for this transducer indicates $\alpha_{-3\text{ dB}}$ = 18.7°, compared to 16.9° from the independent measurements. Due to this large difference, and because Simrad has expressed uncertainty in their angular-measurement accuracy (personal communication, Lars Andersen), the Λ_α of 9.33 electrical°/geometric° estimated for this transducer was applied to data from all of the transducers, resulting in estimates of $\alpha_{-3\text{ dB}}, \beta_{-3\text{ dB}}$, and Ψ that are assumed to be more accurate than those reported by Simrad.

Although these measurements were only made for one transducer in the alongships plane, the estimated Λ_α, 9.33 electrical°/geometric°, was also used for Λ_β and for the alongships and athwartships measurements made with all of the ES38-18 / 200-18C transducers.

Transducer Separation

Using single-target detections of calibrated sphere *TS*, the resulting 38-kHz α_{38} and β_{38} were converted to 200-kHz α_{38} and β_{38} (Eq. 6), and 200-kHz beam-uncompensated TS were fit, using a nonlinear least-squares regression with a bi-square weight function, to the Simrad beam model (**Fig. 8**). This resulted in an estimated transducer spacing, d_α = 15.2 cm.
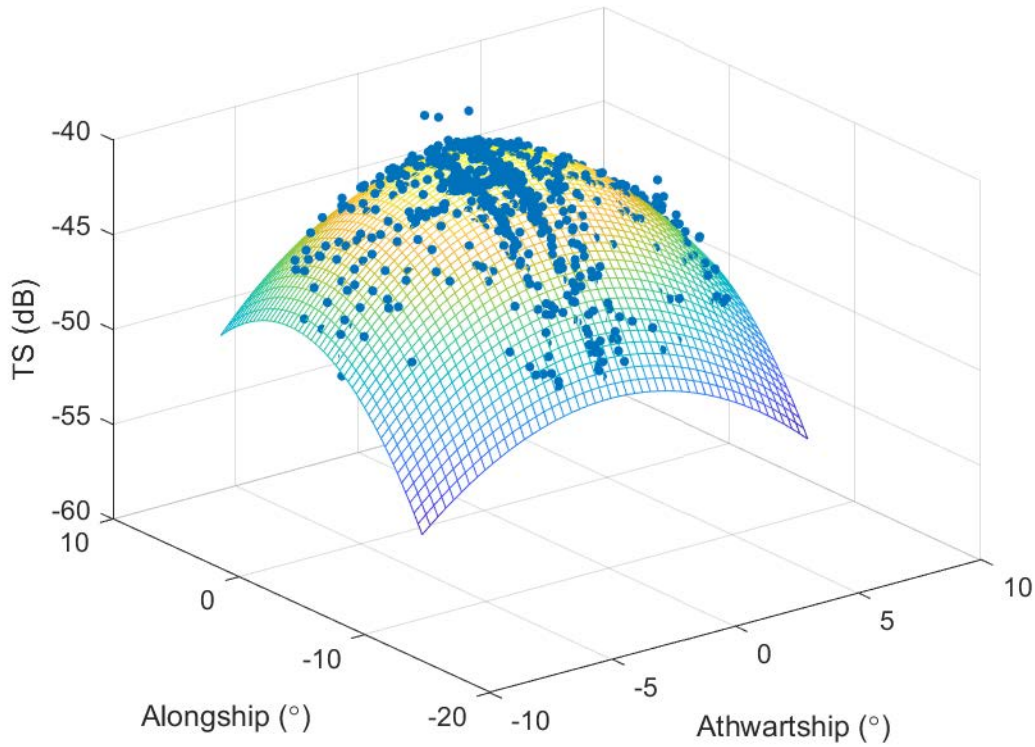

Figure 8. 200-kHz beam-uncompensated TS at target positions derived from the 38-kHz transducer (blue dots), fit to the Simrad beam model (mesh surface). A nonlinear-minimization algorithm was used to estimate the effective transducer spacing.

This d_α was used to convert the 38-kHz target positions to 200-kHz positions (Eq. 6) for the calibrations of each WBT Mini / transducer pair.

Sphere Calibrations

CW

Setting the 38-kHz Λ_α and Λ_β to 9.33 electrical°/geometric°, single target detections for both the 38- and 200-kHz transducers were obtained. The 38-kHz target positions and beam-uncompensated TS data were fit with a nonlinear least-squares regression to obtain estimates of the 38-kHz $TS_{on-axis}$, $\alpha_{-3\,dB}$ and $\beta_{-3\,dB}$, and α_0 and β_0 (**Tables 3 and 4; Fig. 9**):
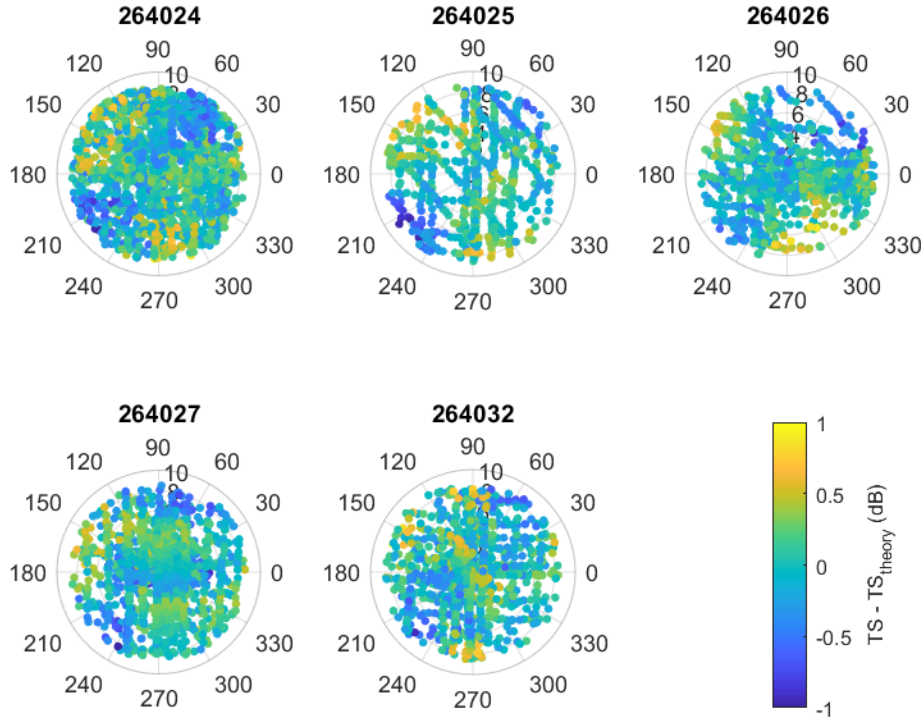
Figure 9. 38-kHz calibrated and beam-compensated TS minus the theoretical TS of a 38.1-mm WC sphere. The beam-uncompensated TS data were fit with the Simrad beam model to derive estimates of transducer gain, beamwidths, and offset angles. The 38-kHz single-target position data was further utilized to estimate target positions in the 200-kHz beam.

The resulting $TS_{\mathrm{on-axis}}$ was used to derive G_0 (Eq. 7) and the $\alpha_{-3\,\mathrm{dB}}$ and $\beta_{-3\,\mathrm{dB}}$ to derive Ψ (Eq. 8). The calibrated G_0, $\alpha_{-3\,\mathrm{dB}}$ and $\beta_{-3\,\mathrm{dB}}$, α_0 and β_0, and Ψ were then used to obtain calibrated TS and S_V. Retaining only those data from which the sphere was on or near the beam axis, a region was then defined around the sphere from which estimates of $S_{V\,\mathrm{mean}}$, T, and r were obtained. $S_{V\,\mathrm{theory}}$ was then calculated (Eq. 9) and the calibrated 38-kHz $S_{a\,\mathrm{corr}}$ was derived (Eq. 10; **Tables 3 and 4**).

The calibrated 38-kHz α_{38} and β_{38} were compensated using d_α = 15.2 cm to obtain estimates of the 200-kHz α_{200} and β_{200} (Eq. 6):
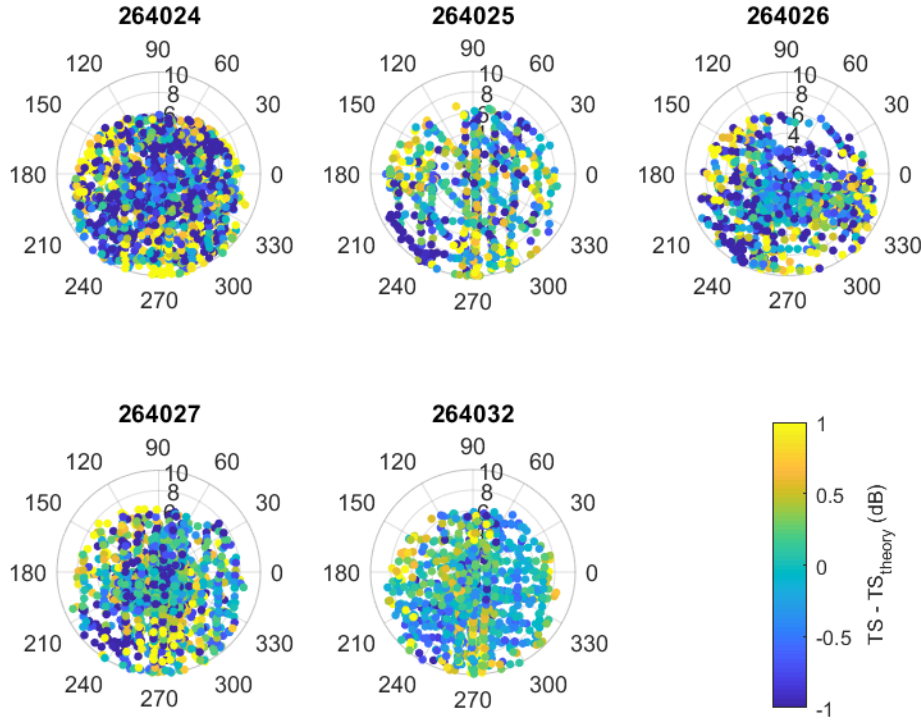
Figure 10. 200-kHz calibrated and beam-compensated TS minus the theoretical TS of a 38.1-mm diameter WC sphere using single-target positions derived from the 38-kHz split-beam data. The beam-uncompensated TS were fit with the Simrad beam model to derive estimates of gain, beamwidths, and offset angles. Because real-time single target detections during the calibration were only available for the 38-kHz transducer, the forward-most portion of the 200-18C, which is forward of the ES38-18, was not mapped with the sphere.

A nonlinear least-squares regression of the 200-kHz α_{200} and β_{200} and beam-uncompensated TS was used to derive 200-kHz $TS_{\text{on-axis}}$, $\alpha_{-3\,\text{dB}}$ and $\beta_{-3\,\text{dB}}$, and α_0 and β_0 (**Tables 3 and 4; Fig. 10**). The resulting $TS_{\text{on-axis}}$ was used to derive G_0 (Eq. 7) and the $\alpha_{-3\,\text{dB}}$ and $\beta_{-3\,\text{dB}}$ to derive Ψ (Eq. 8). The calibrated G_0 and Ψ were then used to obtain calibrated TS and S_V. Retaining only those data from which the sphere was on or near the beam axis, a region was then defined around the sphere from which estimates of $S_{\text{V}\,\text{mean}}$, T, and r were obtained. $S_{\text{V}\,\text{theory}}$ was then calculated (Eq. 9) and the calibrated 200-kHz $S_{\text{a}\,\text{corr}}$ was derived (Eq. 10; **Tables 3 and 4**).

Table 3: Pre-survey calibration results for the 38- and 200-kHz transducers operating in CW mode

-	ES38-18	ES38-18	ES38-18	ES38-18	ES38-18	200-18C	200-18C	200-18C	200-18C	200-18C
Transceiver	264024	264025	264026	264027	264032	264024	264025	264026	264027	264032
Transducer	101	102	103	104	105	101	102	103	104	105

-	ES38-18	ES38-18	ES38-18	ES38-18	ES38-18	200-18C	200-18C	200-18C	200-18C	200-18C
Saildrone	1024	1025	1026	1027	1028	1024	1025	1026	1027	1028
Sound speed (m/s)	1520.91	1520.91	1521.41	1521.41	1521.14	1520.91	1520.91	1521.41	1521.41	1521.14
TS_{theory} **(dB)**	-42.38	-42.38	-42.38	-42.38	-42.38	-38.81	-38.81	-38.81	-38.81	-38.81
G_0 **(dB)**	19.55	18.76	19.41	19.33	19.58	19.21	18.82	19.36	18.75	17.52
$\alpha_{-3\,\text{dB}}$ **(°)**	16.7	17.7	16.4	17.3	16.9	14.4	15.2	14.6	15.1	16.2
$\beta_{-3\,\text{dB}}$ **(°)**	16.7	17.9	16.9	16.9	16.4	13.7	14.8	13.9	14.4	15.0
α_0 **(°)**	0.4	0.0	0.1	-0.2	0.1	-0.1	-0.3	-0.4	-0.3	-0.1
β_0 **(°)**	0.2	0.0	0.1	0.3	-0.3	-0.1	-0.1	0.2	0.2	0.0
Ψ **(dB)**	-13.2	-12.6	-13.2	-13.0	-13.2	-14.7	-14.1	-14.6	-14.3	-13.8
τ_{eff} **(ms)**	0.797	0.797	0.797	0.797	0.797	0.892	0.892	0.892	0.892	0.892
$S_{A\,\text{corr}}$ **(dB)**	0.00	0.02	0.00	0.02	-0.01	0.21	0.03	0.03	0.01	-0.03
RMS	0.17	0.15	0.13	0.16	0.15	0.63	0.41	0.51	0.45	0.27

Table 4: Post-survey calibration results for three of the 38- and 200-kHz transducers operating in CW mode, prior to (transceivers 264025 and 264026) and after (all transceivers) being cleaned of biofouling

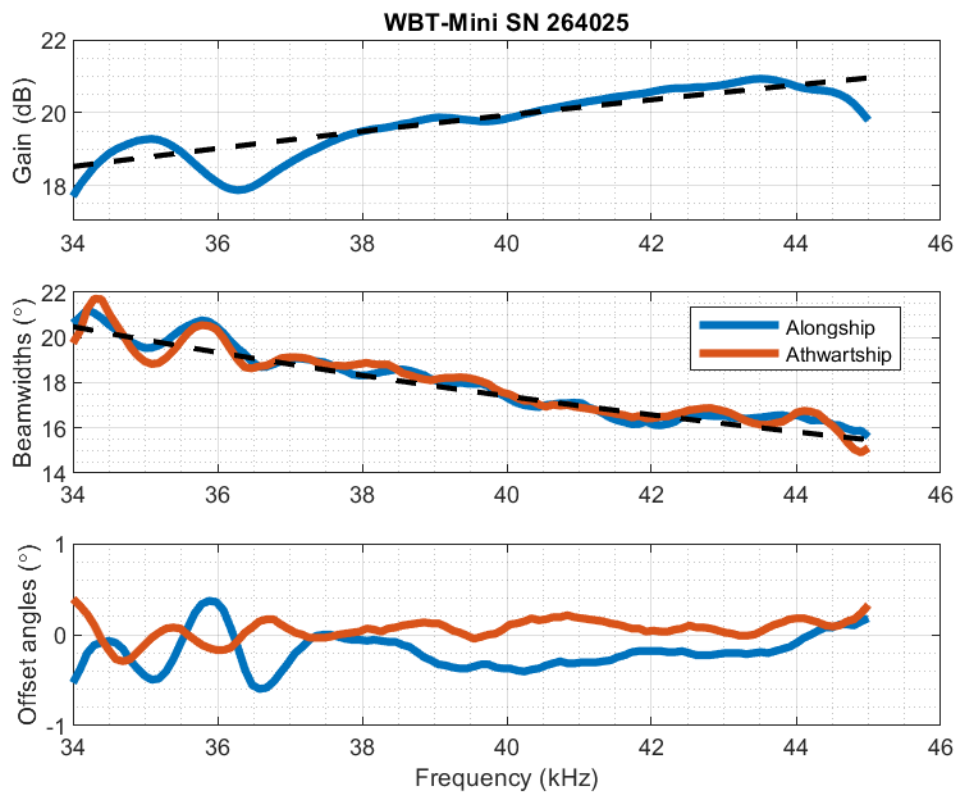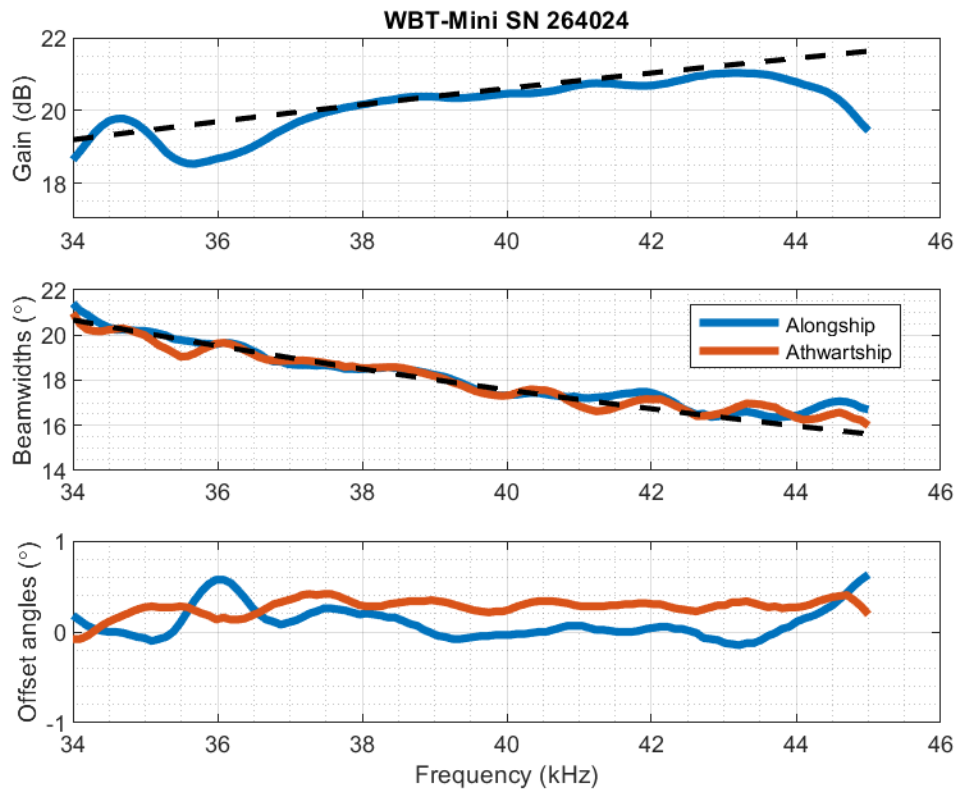| -	ES38-18	ES38-18	ES38-18	ES38-18	ES38-18	200-18C	200-18C	200-18C	200-18C	200-18C
Transceiver	264025	264025	264026	264026	264032	264025	264025	264026	264026	264032
Transducer	102	102	103	103	105	102	102	103	103	105
Saildrone	1025	1025	1026	1026	1028	1025	1025	1026	1026	1028
Biofouling	No	Yes	No	Yes	No	No	Yes	No	Yes	No
Sound speed (m/s)	1518.8	1519.0	1518.8	1520.4	1518.5	1518.8	1519.0	1518.8	1520.4	1518.5
TS_{theory} **(dB)**	-42.39	-42.39	-42.39	-42.38	-42.39	-38.82	-38.82	-38.82	-38.81	-38.83
G_0 **(dB)**	19.12	19.06	19.73	19.67	19.60	19.35	19.29	19.10	19.13	18.97
$\alpha_{-3\,\text{dB}}$ **(°)**	17.7	17.6	16.7	16.7	17.4	18.8	18.3	17.9	17.0	17.7
$\beta_{-3\,\text{dB}}$ **(°)**	18.0	17.5	16.8	16.7	17.6	18.8	18.0	17.5	16.9	17.5
α_0 **(°)**	-0.2	-0.1	-0.2	-0.3	0.0	0.1	-0.2	-0.2	-0.3	0.3
β_0 **(°)**	0.0	0.1	0.1	0.0	-0.5	0.1	0.3	0.3	0.4	0.0
Ψ **(dB)**	-12.6	-12.8	-13.2	-13.2	-12.8	-12.2	-12.5	-12.7	-13.1	-12.7
τ_{eff} **(ms)**	0.797	0.797	0.797	0.797	0.797	0.892	0.892	0.892	0.892	0.892
$S_{A\,\text{corr}}$ **(dB)**	-0.11	-0.04	-0.10	0.00	-0.02	-0.01	-0.02	-0.01	-0.08	-0.03
RMS	0.17	0.15	0.15	0.15	0.16	0.17	0.16	0.16	0.16	0.17

For the ES38-18 transducers, values of pre-survey G_0 ranged from 18.8 (SN 264025) to 19.6 dB re 1 (SN 264024 and SN 264032). Post-survey values ranged from 19.1 (SN 264025) to 19.7 dB re 1 (SN 264026). For the post-survey calibrations with and without biofouling, values of G_0 varied ≤0.1 dB re 1 and Ψ varied ≤0.2 dB re 1 sr. The beam-model fits had RMS ≤ 0.17 dB re 1.
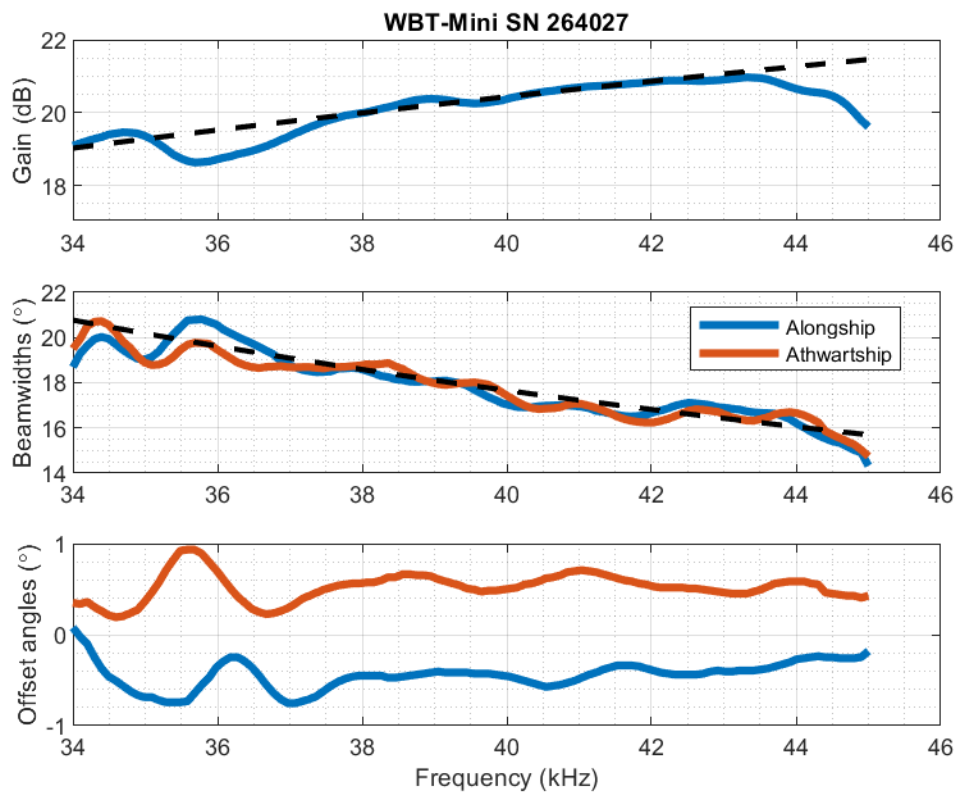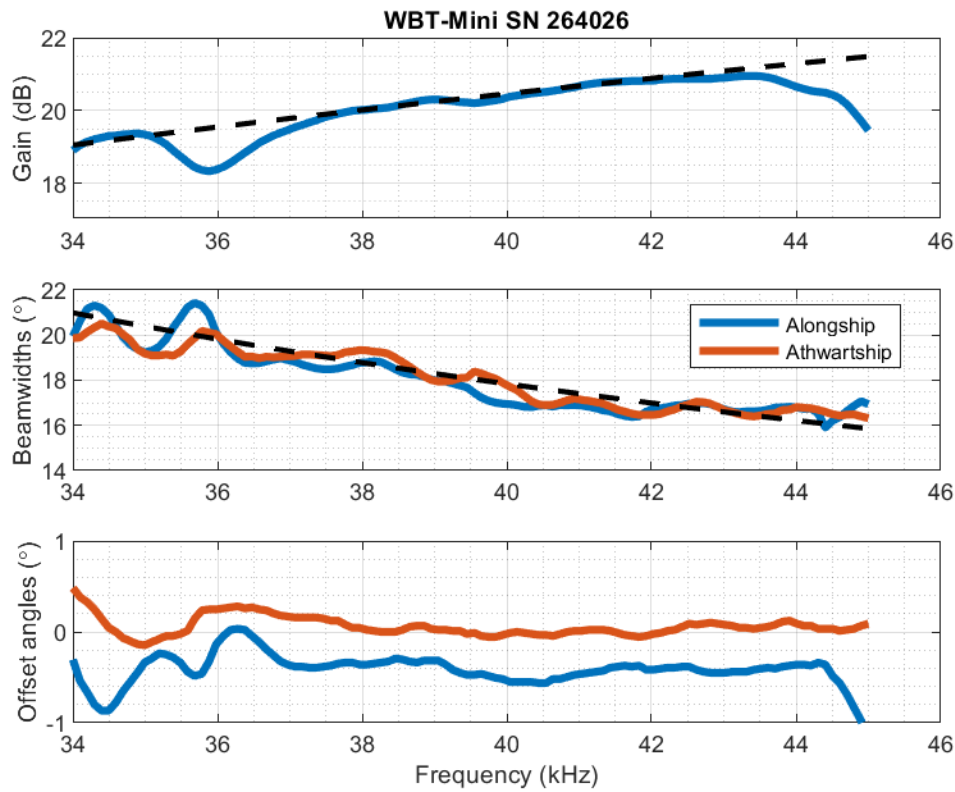
For the 200-18C transducers, values of pre-survey G_0 ranged from 17.5 (SN 264032) to 19.4 dB re 1 (SN 264026). Post-survey values ranged from 19.0 (SN 264032) to 19.4 dB re 1 (SN 264025). For the post-survey calibrations with and without biofouling, values of G_0 varied ≤0.1 dB re 1 and Ψ varied ≤0.4 dB re 1 sr. The pre-survey beam-model fits had RMS ranging from 0.27 to 0.63 dB, compared to the post-survey values ranging from 0.16 to 0.17 dB.

For the three systems calibrated before and after the survey (SN 264025, SN 264026, and SN 264032), the ES38-18 G_0 changed by 0.3, 0.3, and 0.0 dB re 1 and the 200-18C by 0.6, -0.3, and 1.5 dB re 1, respectively; and the ES38-18 Ψ changed by ~-0.1, 0.0, and 0.4 dB re 1 sr and the 200-18C by ~1.7, 1.7, and 1.1 dB re 1 sr, respectively.

FM

38-kHz FM data was processed using the EK80 calibration utility to derive estimates of calibrated G_0, $\alpha_{-3\,\text{dB}}$ and $\beta_{-3\,\text{dB}}$, and α_0 and β_0 across the FM spectra. The $\alpha_{-3\,\text{dB}}$ and $\beta_{-3\,\text{dB}}$, and α_0 and β_0 were then compensated by the change in Λ_α and Λ_β (Eq. 5). Comparisons were made to the theoretical change in G_0, $\alpha_{-3\,\text{dB}}$ and $\beta_{-3\,\text{dB}}$ versus frequencies (Eqs. 12 and 13; **Fig. 11**).

WBT-Mini SN 264024

WBT-Mini SN 264025

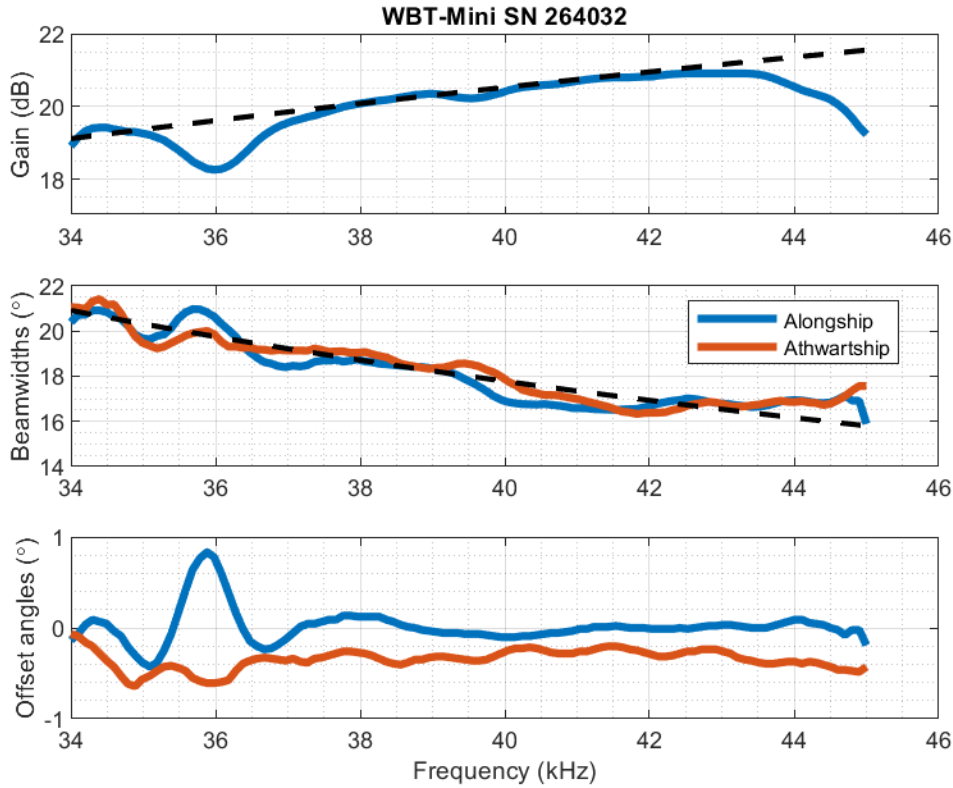WBT-Mini SN 264026

WBT-Mini SN 264027

Figure 11. FM calibration results for the 38-kHz transducers, obtained from the EK80 calibration utility. The resulting beamwidths and offset angles were compensated by the difference in the calibrated and default angle sensitivities. Included are theoretical changes in gain and beamwidths versus frequency (dashed black lines).

Discussion

Aside from actual changes in the transducer performance, some of the variations in the calibration results may be due to differences between the pre- and post-survey calibration procedures: (1) the transducer depth was ~0.7 and 2 m below the water surface, respectively, potentially placing the transducers in stratified, lower-salinity water during the pre-survey calibrations; (2) in the pre-survey calibrations, the sphere was suspended via a single monofilament loop glued into a spark-eroded hole, whereas the post-survey calibrations had the sphere suspended in a net bag made of braided Dyneema; and (3) prior to the post-survey calibrations, the pitch motor was rotated ~80°, positioning the transducer approximately horizontal and shedding any potential bubbles on the transducer face.

Considering the differences in pre- and post-survey calibration procedures, the general increase in G_0, and the decrease in RMS values, the post-survey calibration results are likely more accurate. In any case, the pre- and post-survey calibration results did not change significantly for the ES38-18 (≤ 0.4 dB). However, for the 200-18C transducers, because the pre-survey

RMS was large and estimates of Ψ changed significantly between the pre- and post-survey calibrations (up to 1.7 dB), use of the pre-survey calibration results may result in larger measurement uncertainties.

Recommendations

Because the EK Mission Planner software does not currently allow for more than one frequency to transmit when using the calibration utility, it was necessary to collect calibration data by programming and activating a mission plan. In this mode, real-time single target positions were not available during the calibration. This made it difficult to ensure that both the 38- and 200-kHz beams were being sufficiently mapped, as evidenced by the lack of single target detections in the forward-most section of the 200-kHz beam (**Fig. 10**). If the calibration utility allowed the transmission of multiple frequencies simultaneously, while having single target positions available for at least one transducer, calibration time would be reduced and more comprehensive datasets would improve the calibration results.

The estimate of $d_\alpha = 15.2$ cm for the 38- and 200-kHz transducer spacing was derived for transducer SN 105 and applied to all other transducers. If d_α varies among transducers, the 200-kHz target positions derived from data collected with the other transducers could have additional error. This error would propagate to the estimates of G_0, $\alpha_{-3\,\mathrm{dB}}$ and $\beta_{-3\,\mathrm{dB}}$, and Ψ for each transducer. Measurements of d_α for each of the transducers would characterize any variation in this value among transducers, which could reduce calibration uncertainty.

The Λ_α derived from measurements with the ES38-18/200-18C transducer (SN 105) were used for both the Λ_α and Λ_β for all of the transducers. If the Λ_α and Λ_β vary, and among transducers, the estimated $\alpha_{-3\,\mathrm{dB}}$ and $\beta_{-3\,\mathrm{dB}}$ for the other 200-kHz transducers could have additional error. To sequentially measure Λ_α and Λ_β, the transducer could be rotated 90° on the pitch tray. Alternatively, the pole could be lowered such that the transducer is 5 m below the water surface, projecting horizontally, and the transducer pitched and then rotated. Either approach could be repeated for each of the transducers.

The EK80 software (V 1.12.2) does not allow modifications of the Ψ nor Λ_α and Λ_β, except for editing a low-level XML file, which is not recommended. Moreover, changes to these parameters cannot be made when replaying raw data, despite having no effect on the underlying data. To apply calibrated values of these parameters for deriving $\alpha_{-3\,\mathrm{dB}}$ and $\beta_{-3\,\mathrm{dB}}$, α_0 and β_0, and $S_{a\,\mathrm{corr}}$, it was necessary to process the data externally, in this case using Echoview and Matlab. Although the EK80-derived $\alpha_{-3\,\mathrm{dB}}$ and $\beta_{-3\,\mathrm{dB}}$, and α_0 and β_0 can be compensated by the change in Λ_α and Λ_β (Eq. 6), it would be better to update the Ψ and Λ_α and Λ_β and replay data in the calibration utility.

An external program is needed to localize the 200-kHz single-target detections using the 38-kHz α and β and an estimate of the d_α. This too, could be implemented in the EK80 software.

A fourth system (WBT-Mini 264024) was to be re-calibrated after the survey, however while operating the transceiver the regulated power supply (Agilent E3634A) tripped due to an over-voltage protection fault. Subsequently, the transceiver was inoperable. The WBT-Minis should have improved input-power protections.

References

Bodholt, H., 2002. The effect of water temperature and salinity on echo sounder measurements. ICES Symposium on Acoustics in Fisheries, Montpellier, Paper No. 123

Demer, D.A., Soule, M.A. and Hewitt, R.P., 1999. A multiple-frequency method for potentially improving the accuracy and precision of in situ target strength measurements. *The Journal of the Acoustical Society of America*, *105*(4), pp.2359-2376.

Demer, D.A., Berger, L., Bernasconi, M., Bethke, E., Boswell, K., Chu, D., Domokos, R., Dunford, A., Fässler, S., Gauthier, S. and Hufnagle, L.T., 2015. Calibration of acoustic instruments. ICES Cooperative Research Report, 326.

Demer, D. A., Cutter, G. R., Stierhoff, K. L., and Renfree, J. S., 2015. Two-Million-Liter Tank Expands the Boundaries of Marine Technology Innovation: National Resource Available for Advancing Marine Science. Marine Technology Society Journal 49(2), pp.87-98.

Demer, D.A., Andersen, L.A., Bassett, C., Berger, L., Chu, D., Condiotty, J., Cutter, G.R., Hutton, B., Korneliussen, R., Le Bouffant, N., Macaulay, G., Michaels, W.L., Murfin, D., Pobitzer, A., Renfree, J.S., Sessions, T.S., Stierhoff, K.L., and Thompson, C. H., 2017. Evaluation of a wideband echosounder for fisheries and marine ecosystem science. ICES Cooperative Research Report, 336.

Foote, K. G., Knudsen, H. P., Vestnes, G., MacLennan, D. N., and Simmonds, E. J., 1987. Calibration of acoustic instruments for fish density estimation: A practical guide. Cooperative Research Report 144, International Council for the Exploration of the Sea, Copenhagen, Denmark, 69 pp.

Korneliussen, R. J., Diner, N., Ona, E., Berger, L., and Fernandes, P. G. 2008. Proposals for the collection of multifrequency acoustic data. ICES Journal of Marine Science, 65: 982–994.

MacLennan, D. N., Fernandes, P. G., and Dalen, J. 2002. A consistent approach to definitions and symbols in fisheries acoustics. ICES Journal of Marine Science, 59: 365– 369.

Urick, R. J. 1983. Principles of Underwater Sound, 3rd edn. McGraw-Hill, New York.